JOURNAL OF SPACECRAFT AND ROCKETS
Vol. 45, No. 3, May–June 2008

New Methods to Predict Nonlinear Pitch Damping Moments

F. G. Moore* and L. Y. Moore†
Aeroprediction, Inc., King George, Virginia 22485

DOI: 10.2514/1.33745

Two new methods have been developed to approximate pitch damping as a function of both angle of attack and Mach number. The new methods can be used over the Mach number (0–20) and angle-of-attack range (0–90 deg) of the Aeroprediction Code. The first method is based on the static nonlinear loads on the body and lifting surfaces that are available in the Aeroprediction Code. The second method is based on the improved linear value of pitch damping that was recently developed for the Aeroprediction Code. Recent improvements to the linear value include accuracy improvements for configurations with long boattails and double counting of the body length beneath a lifting surface. A method was derived to relate the zero angle-of-attack value of the pitch damping to a nonlinear value at an angle of attack. Comparison of the two new methods to experimental data shows that both methods give results which follow the trends of experimental data, but neither method is superior for all cases at all angles of attack. As a result, results for both methods will be computed and available to the user of the Aeroprediction Code. The new methods will be a part of the 2009 version of the Aeroprediction Code, the AP09.

Nomenclature

A_{ref}	=	reference area (maximum cross-sectional area of body, if a body is present, or planform area of wing, if wing alone), ft^2
A_W	=	wing planform area, ft^2
C_M	=	pitching moment coefficient (based on reference area and body diameter, if body present, or mean aerodynamic chord, if wing alone)
C_{M_B}, C_{M_T}	=	pitching moment coefficient of body or tail alone, respectively
$C_{M_q} + C_{M_{\dot\alpha}}$	=	pitch damping moment coefficient $[C_M(q)/(qd/2V_\infty) + C_M(\dot\alpha)/(\dot\alpha d/2V_\infty)]$
C_{M_α}	=	pitching moment coefficient derivative (per radian)
C_N	=	normal-force coefficient
C_{N_B}	=	normal-force coefficient of body alone
C_{N_W}	=	normal-force coefficient of wing alone
$C_{N_{C(B)}}$, $C_{N_{W(B)}}$, $C_{N_{T(B)}}$	=	normal-force coefficient of canard, wing, or tail in presence of body
$C_{N_{T(V)}}$	=	normal-force coefficient on tail as a result of wing shed vortices
C_{N_α}	=	normal-force coefficient derivative (per radian)
C_P	=	pressure coefficient
d_{ref}	=	reference body diameter, ft
I_y	=	moment of inertia about the pitch plane, lb · ft^2
$K_{W(B)}$, $k_{W(B)}$	=	ratio of normal-force coefficient of wing or tail in presence of body to that of wing or tail alone at $\delta = 0$ deg or $\alpha = 0$ deg, respectively
M, M_α	=	pitching moment and pitching moment slope, respectively, ft · lb
M_L, M_∞	=	local or freestream Mach number, respectively
N_B	=	normal force of body alone, lb
$N_{B(C)}$, $N_{B(W)}$	=	additional normal force on body as a result of canard or wings, respectively, lb
$N_{C(B)}$, $N_{W(B)}$	=	normal force on canard or wing, respectively, in presence of body, lb
N_{CW}	=	normal force on wing or tail due to canards, lb
P_L, P_∞	=	local and freestream pressure, respectively
Q_L, Q_∞	=	local or freestream dynamic pressure, lb/ft^2
q	=	pitch rate, rad/s
R_N	=	Reynolds number
r	=	local body radius
s	=	local body radius plus wing semispan
T_L, T_∞	=	local and freestream temperature, respectively
V_∞, V_L	=	freestream and local velocity, respectively
W	=	running load, lb/ft
X	=	distance from nose tip, ft
X_{CG}	=	distance to center of gravity, ft
X_{CP}	=	center of pressure (in feet or calibers from some reference point that can be specified) in x direction
X_{CP}/d	=	center of pressure (calibers from some reference point)
X_{LE}, X_{AFT}	=	distance from nose tip to wing leading edge or afterbody, respectively, (in ft or calibers from point that can be specified)
α	=	angle of attack, deg
γ	=	ratio of specific heats
$\Delta C_{N_{B(C)}}$, $\Delta C_{N_{B(W)}}$, $\Delta C_{N_{B(T)}}$	=	additional normal-force coefficient on body in presence of canard, wing, or tail
μ	=	damping constant, lb · ft^2/s
ρ_∞	=	freestream density, lb/ft^3
Φ	=	roll position of missile fins [$\Phi = 0$ deg corresponds to fins in the plus (+) orientation. $\Phi = 45$ deg corresponds to fins rolled to the cross (×) orientation]

Presented at the 46th AIAA Aerospace Sciences Conference, Reno, NV, 7–10 January 2008; received 27 July 2007; revision received 26 September 2007; accepted for publication 27 September 2007.

*President; drfgmoore@hotmail.com. Associate Fellow AIAA.
†Computer Scientist.

Introduction

ONE area that has basically remained the same since the 1977 version of the Aeroprediction Code (AP77) is the linearity of the dynamic derivatives. Nonlinear static aerodynamics were first incorporated into the code in 1993 up to angle of attack (AOA) of 30 deg. The nonlinear static aerodynamics were extended to 90 deg AOA in 1995 and to the roll position of 45 deg in 1998. The nonlinear

static aerodynamics were then improved upon with the AP02 based on a new wind-tunnel database that varied r/s. The static aerodynamic nonlinearities are well documented in [1,2].

Unfortunately, no such generic wind-tunnel databases exist for dynamic derivatives as exist for static aerodynamics. In researching the literature, several pieces of dynamic derivative wind-tunnel data were available for various configurations. These wind-tunnel and ballistic range data ([3–18]) are all for a specific configuration at a limited number of Mach numbers and AOAs. References [3–12] are all open literature whereas [13–18] are unclassified, but limited distribution.

The wind-tunnel data of [3–18] were generally taken by one of three methods. The first approach (pioneered in the late 1950s and early 1960s) at the then Naval Ordnance Laboratory (NOL), White Oak, Maryland [now part of Arnold Engineering Development Center (AEDC)], was to place a steel rod through the center of gravity (CG) of the model and attach it to the wind-tunnel walls. The model was then deflected to a certain AOA and the damping motion was recorded in both time and AOA. This type of testing was referred to as "free oscillation" and required the model to be statically stable. For large AOA, the damping derivatives were measured in increments of AOA decay (see [3], for example), and the pitch damping moment was determined from the linearized equation:

$$I_y\ddot{\alpha} + \mu\dot{\alpha} + M_\alpha\alpha = 0 \tag{1}$$

Equation (1), while linear, was assumed to apply over increments in AOA, even though the C_{M_α} and μ (the damping constant) may be different from increment to increment. That is, for the increment of interest, C_{M_α} and μ were assumed constant.

A second type of pitch damping test for small to moderate AOAs was performed at AEDC [17], where a sting was attached to the model and the model was forced to oscillate about 3 deg AOA range. This type of mechanism could determine pitch damping for stable or unstable configurations. The sting and model were moved to a certain AOA and a forced oscillation of ± 3 deg in AOA was performed by the sting on the model and the decay of the model measured. This type of testing is referred to as "forced oscillation testing."

A third type of pitch damping test for high AOA was also performed at AEDC where a strut was mounted to the leeward plane of the model [4]. A similar forced oscillation system was used to record the damping derivatives as in method 2 discussed previously. However, here due to the strut mounting technique, AOAs to 90 deg can be achieved.

Fundamentally, the first and third types of testing have issues of wind-tunnel wall or model installation interference issues or both. The pitch damping tests performed in the late 1950s and early 1960s at NOL were in a small test section with a model that had a rod going through the center of gravity. Thus wall interference and rod interference on the damping characteristics are both issues. The strut used in the high AOA testing is quite thick and definitely will influence aerodynamics behind the strut. The second type of pitch damping testing is similar to static aerodynamic testing and should have minimal wind-tunnel interference. Unfortunately, most of the databases at AOA in the open literature have used either test technique 1 or 3. As a result, development of a nonlinear semi-empirical pitch damping model will be based on a meager amount of data that unfortunately has more wind-tunnel interference issues associated with the data than is desired. Ballistic range data help to validate wind-tunnel data at low AOA but are of no help at moderate to high AOA.

New Improvements for AP09

The literature survey ([3–18]) did not produce any analytical methods to predict nonlinear pitch damping. This is not surprising given the meager amount of nonlinear data. Hence, the methods discussed in this paper are, to the authors' knowledge, the first attempt to predict nonlinear pitch damping moments.

Three methods will be investigated for predicting nonlinear pitch damping moments. Two of the methods are either new or improved upon state-of-the-art methods. Also, two of the methods are based strictly on the static aerodynamics whereas the third method is based on the improved zero AOA pitch damping method of the AP09 discussed in [19]. Each of the three different methods will now be discussed individually.

The first two methods are based on more generalized methods of [20], Chapter 9. The total normal force for a wing–body–tail configuration can be defined by

$$C_N = C_{N_B} + C_{N_{W(B)}} + \Delta C_{N_{B(W)}} + C_{N_{T(B)}} + \Delta C_{N_{B(T)}} + C_{N_{T(V)}} \tag{2}$$

Using the Ref. [20] analogy, the pitch damping moment is thus

$$\begin{aligned} C_{M_q} + C_{M_{\dot\alpha}} = {} & (C_{N_\alpha})_B \left(\frac{X_{\mathrm{CP}} - X_{\mathrm{CG}}}{d}\right)^2_B \\ & + (C_{N_\alpha})_{W(B)} \left(\frac{X_{\mathrm{CP}} - X_{\mathrm{CG}}}{d}\right)^2_{W(B)} + (\Delta C_{N_\alpha})_{B(W)} \left(\frac{X_{\mathrm{CP}} - X_{\mathrm{CG}}}{d}\right)^2_{B(W)} \\ & + (C_{N_\alpha})_{T(B)} \left(\frac{X_{\mathrm{CP}} - X_{\mathrm{CG}}}{d}\right)^2_{T(B)} + (\Delta C_{N_\alpha})_{B(T)} \left(\frac{X_{\mathrm{CP}} - X_{\mathrm{CG}}}{d}\right)^2_{B(T)} \\ & + (C_{N_\alpha})_{T(V)} \left(\frac{X_{\mathrm{CP}} - X_{\mathrm{CG}}}{d}\right)^2_{T(V)} \end{aligned} \tag{3}$$

Before proceeding to use Eq. (3), discussion of the nonlinearities in the Aeroprediction Code (APC) to predict each of the static aerodynamic terms of Eq. (3) is appropriate. As an example, consider the term $C_{N_{W(B)}}$ of Eq. (2) which can be expanded as follows:

$$C_{N_{W(B)}} = \lfloor K_{W(B)} \sin\alpha + k_{W(B)} \sin\delta \rfloor (C_{N_\alpha})_W \tag{4}$$

Each of the terms in Eq. (4), $K_{W(B)}$, $k_{W(B)}$, and $(C_{N_\alpha})_W$, are nonlinear in AOA or control deflection and Mach number. The nonlinearities were based on several large wind-tunnel databases in addition to other missile data [1,2]. As an example of the nonlinearities, consider the wing–body interference term $K_{W(B)}$. $K_{W(B)}$ is typically close to the slender body theory value at zero AOA and at all Mach numbers. However, at low Mach number, as α increases, $K_{W(B)}$ will typically decrease to a value of 1.0 at high AOA. On the other hand, as Mach number increases, $K_{W(B)}$ will approach 1 at fairly low AOAs.

Not only are the normal-force coefficient terms of Eq. (2) all nonlinear, but the center of pressure terms of Eq. (3) as well. For a complete description of the static aerodynamic nonlinearities in the Aeroprediction Code, [1,2] should be consulted.

The first approach taken to predict nonlinear pitch damping moments was to use Eq. (3) directly where all the terms in Eq. (3) are the nonlinear aerodynamic terms computed in the AP09. Figure 1 compares the results of method 1 to experimental data for the Army–Navy–Finner (ANF) of [3,4,12]. Note that method 1 compares quite well to data at low AOA but actually decreases with AOA versus increases as the data suggest. In investigating why method 1 decreases with increasing AOA, it was found that the body–wing and wing–body interference terms decreased with AOA, which tended to somewhat compensate for the increase in wing alone normal force. Secondly, it was found that when treating the body as a point source, the body center of pressure moved toward the center of gravity as AOA increased, thus causing the term $[(X_{\mathrm{CP}} - X_{\mathrm{CG}})/d]^2_B$ to decrease. As a result of the disappointing results of method 1 in Fig. 1, it will not be considered any further and other approaches will be attempted.

A logical extension of method 1 is to distribute the load along the body, as opposed to treating the body as a point source. The structural load methodology [21] of the AP09 code will be used to perform this task. To illustrate the structural load methodology of the AP09, Fig. 2 shows the AP09 loads at $M_\infty = 2.87$, $\Phi = 45$ deg, and $\alpha = 10$ deg compared to Navier–Stokes computations for a wing–body–tail configuration. There are two aeroprediction results in Fig. 2, original and adjusted. The adjusted curve takes part of the nose overprediction on load and redistributes it while still maintaining accuracy of normal-force and pitching moments. The increase in load on the mid- and aftbody areas of Fig. 2 is the wing–body carryover normal-force distribution. The major point of Fig. 2 is to illustrate the

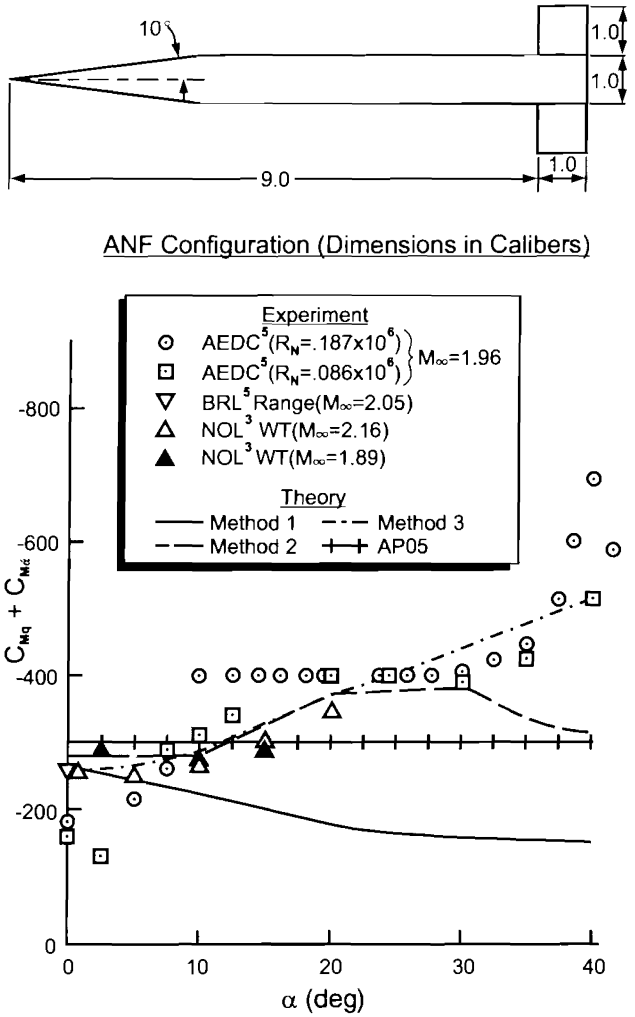

Fig. 1 Comparison of various theoretical approaches to predict nonlinear pitch damping moment to experimental data for the ANF.

accuracy of the Aeroprediction Code in calculating loads on a body, which can be important in predicting pitch damping moments.

Figure 3 now illustrates the local loads on two more relevant configurations where nonlinear pitch damping moment data are available, the ANF and the (MK 82) general purpose low drag bomb (GPLDB) [8,9]. The ANF is shown on the left of Fig. 3 along with local loads at $\Phi = 0$, $M = 2.16$, and $\alpha = 5$ and 35 deg and the GPLDB is on the right of Fig. 3 along with local loads at $\Phi = 0$, $M = 1.5$, and α of 5 and 35 deg. Note that load distributions of the ANF are similar at 5 and 35 deg as are the loads on the GPLDB at 5 and 35 deg. Of course, the loads at 35 deg are much higher than those at 5 deg. It is also worth noting the negative load on the boattail area of the GPLDB. Returning to Eq. (3), it is seen that as the center of pressure of the overall normal-force load of Figs. 2 and 3 moves toward the center of gravity, the moment arm gets smaller and thus according to Eq. (3), the pitch damping term of the body goes down substantially. This is a prime reason for method 1 of Fig. 1 decreasing as α increases as opposed to increasing as the experimental data suggest.

Robinson in [15], on the other hand, obtains body-alone pitch damping through a summation of local normal force on a body component where the body is divided into 20 parts. In viewing Figs. 2 and 3, it is clearly seen that using an average of center of pressure is not acceptable because the average is a linear average, whereas Eq. (3) has a square of the distance to each of the body parts, whether the body is 20 or more parts. It is also seen in viewing the GPLDB of Fig. 3 that the boattail will decrease the pitch damping moment because the C_{N_α} of the local body normal-force component in the boattail region is negative. In other words, one cannot use the overall nonlinear body center of pressure to compute body pitch damping as AOA increases, as was done in method 1 of Fig. 1.

Method 2 of Fig. 1 uses the summation approach of [15] to compute the pitch damping moment. Using the local load $W(X)$ of Fig. 3, the pitch damping moment for a body–tail configuration is

$$C_{M_q} + C_{M_\alpha} = \frac{-2}{\sin\alpha}\left[\sum_{i=1}^{N}\frac{W(X_i)\Delta X_i}{Q_\infty A_{\text{ref}}}\left(\frac{X_i - X_{\text{CG}}}{d_{\text{ref}}}\right)^2_B + C_{N_{W(B)}}\left(\frac{X_{\text{CP}} - X_{\text{CG}}}{d_{\text{ref}}}\right)^2_{W(B)}\right] \tag{5}$$

Equation (5) was used to compute pitch damping on the ANF at $M_\infty = 2.0$, where $W(X_i)$, $C_{N_{W(B)}}$ and $(X_{\text{CP}})_{W(B)}$ were all nonlinear values from the AP09. Also, body–wing interference is included in the body pitch damping integration since it is included in the body loads. As seen in Fig. 1, method 2 is much better than method 1 and agrees with the NOL and Ballistics Research Laboratory (BRL) data quite well but falls below the AEDC data. A couple of points need to be made about the method 2 results of Fig. 1. First, it was found that the AP09 code needed to be modified to compute local values of C_{N_α} versus the secant slope of C_{N_α}, which is what the AP05 does. Secondly, it was found the overall configuration C_{N_α} gave slightly improved results compared to using individual C_{N_α} values of $C_{N_{W(B)}}$ and C_{N_B}. Thirdly, Eq. (5) assumes the lifting surface is a point source as opposed to distributing the load analogous to the body. In checking out the validity of treating the wing or canards as a point source, it was found that when the root chord was small compared to the body length, small errors typically occurred for the pitch damping term of the lifting surface. However, when the root chord was large compared to the body length, errors in pitch damping could be fairly large. As a result, the load on both the forward and aft lifting surfaces will be divided into 100 equal chordwise intervals. Equation (5) then becomes for a body–tail case:

$$C_{M_q} + C_{M_\alpha} = \frac{-2}{\sin\alpha}\left[\sum_{i=1}^{N}\frac{W(X_i)\Delta X_i}{Q_\infty A_{\text{ref}}}\left(\frac{X_i - X_{\text{CG}}}{d_{\text{ref}}}\right)^2_B + 2C_{N_{W(B)}}\sum_{i=1}^{100}\left(\frac{(X_{\text{CP}})_i - X_{\text{CG}}}{d_{\text{ref}}}\right)^2_{W(B)}\frac{(A_W)_i}{A_W}\right] \tag{5a}$$

Equation (5) is, of course, generalized in the APC for a wing–body tail in a similar fashion as Eq. (3). Also $(A_W)_i$ of Eq. (5a) is the area of the individual wing panel compared to the wing area of a single wing, $A_W/2$ and thus the factor of 2 for the wing–body term.

The third method shown in Fig. 1 uses the improved pitch damping moment improvements discussed in [19] and relates the improved zero AOA pitch damping to the local conditions at a higher AOA. In reviewing [20] in more detail, the pitch damping moment was derived based on the assumption that the local velocity and dynamic pressure at a point on the body or tail fin was the same as the freestream values so that the dynamic pressure Q would cancel out when nondimensionalizing the moment equation to obtain the pitching moment. That is, the pitching moment for a wing–body–tail configuration about some reference point is

$$M = -[N_B(X_{\text{CP}} - X_{\text{ref}})_B + (N_{C(B)} + N_{B(C)})(X_{\text{CP}} - X_{\text{ref}})_C + (N_{W(B)} + N_{B(W)})(X_{\text{CP}} - X_{\text{ref}})_W + N_{\text{CW}}(X_{\text{CP}} - X_{\text{ref}})_W] \tag{6}$$

Equation (6) can be rewritten in coefficient form as

$$C_M = -\frac{Q_L}{Q_\infty}\left[C_{N_B}\left(\frac{X_{\text{CP}} - X_{\text{ref}}}{d_{\text{ref}}}\right)_B + (C_{N_{C(B)}} + C_{N_{B(C)}})\left(\frac{X_{\text{CP}} - X_{\text{ref}}}{d_{\text{ref}}}\right)_C + (C_{N_{W(B)}} + \Delta C_{N_{B(W)}} + C_{N_{CW}})\left(\frac{X_{\text{CP}} - X_{\text{ref}}}{d_{\text{ref}}}\right)_W\right] \tag{7}$$

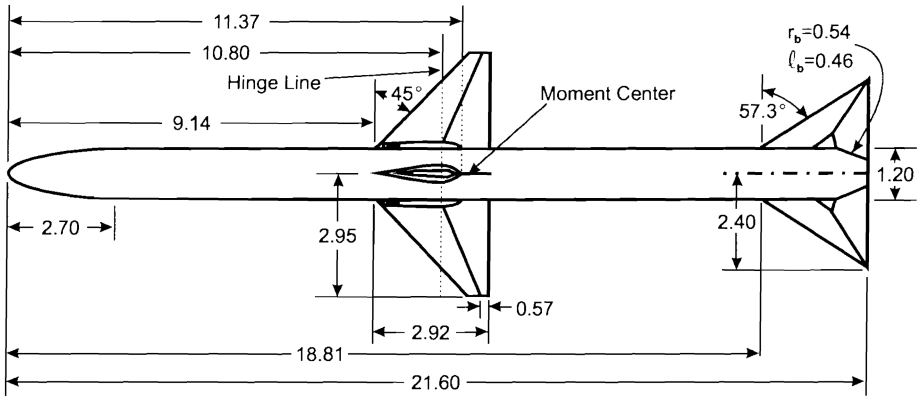

Wing-Body-Tail Configuration Used In Structural Loads Methodology (dimensions In Inches)

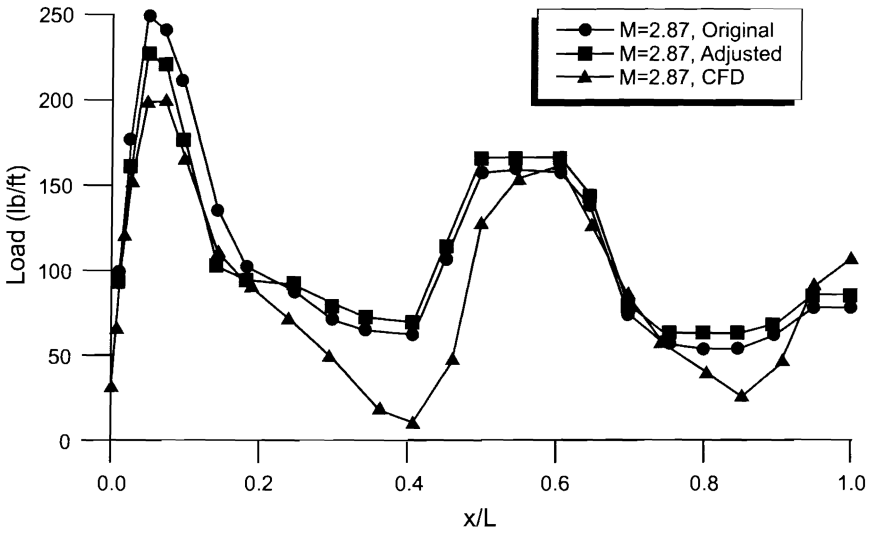

Effect of adjustment of nonlinear component of nose load Φ=45°, α=10°

Fig. 2 Illustration of local load on a wing–body–tail configuration.

Equation (7) assumes all normal-force coefficient terms have been referenced to the appropriate reference areas for simplicity.

Furthermore, putting Eq. (7) in slope form on the right side and using only the tail term for simplicity we have

$$C_{M_T} = -\frac{Q_L}{Q_\infty}[(C_{N_\alpha})_{W(B)} + (\Delta C_{N_\alpha})_{B(W)} + (C_{N_\alpha})_{CW}]\left(\frac{X_{\text{CP}} - X_{\text{ref}}}{d_{\text{ref}}}\right)_T \Delta\alpha_T \tag{8}$$

where

$$\Delta\alpha_T \cong \frac{q}{V_L}\left(\frac{X_{\text{CP}} - X_{\text{ref}}}{d_{\text{ref}}}\right)_T \tag{9}$$

Now $C_{M_Q} = \partial C_M/\partial(qd/2V_\infty)$, so Eq. (8) becomes, after substituting in Eq. (9) and taking the derivative,

$$(C_{M_Q})_T = -2[(C_{N_\alpha})_{W(B)} + (\Delta C_{N_\alpha})_{B(W)} + (C_{N_\alpha})_{CW}]\left(\frac{X_{\text{CP}} - X_{\text{ref}}}{d_{\text{ref}}}\right)^2 \frac{Q_L}{Q_\infty}\frac{V_\infty}{V_L} \tag{10}$$

Equation (10) applies only to the tail term but the factor

$$\frac{Q_L V_\infty}{Q_\infty V_L} \tag{11}$$

would multiply all terms of Eq. (7) if expanded similarly to Eq. (10). We will now look at defining the Eq. (11) term.

Now

$$\frac{Q_L}{Q_\infty} = \frac{\frac{1}{2}\rho_L V_L^2}{\frac{1}{2}\rho_\infty V_\infty^2} = \left(\frac{P_L}{T_L}\right)\left(\frac{V_L^2}{V_\infty^2}\right)\left(\frac{T_\infty}{P_\infty}\right) \tag{12}$$

But

$$C_p = \frac{P_L - P_\infty}{\frac{1}{2}\rho_\infty V_\infty^2} \tag{13}$$

So that

$$P_L = \tfrac{1}{2}\rho_\infty V_\infty^2 C_p + P_\infty \tag{14}$$

Using Eq. (14) into (12) we have

$$\frac{Q_L}{Q_\infty} = \left(\frac{V_L}{V_\infty}\right)^2\left(\frac{T_\infty}{T_L}\right)\left(\frac{\gamma M_\infty^2}{2}C_p + 1\right) \tag{15}$$

Now we will make a couple of approximations where

$$V_L \cong V_\infty \cos\alpha \tag{16}$$

$$C_p = 2\sin^2\alpha \tag{17}$$

Equation (17) is the Newtonian flow approximation which in principal is derived based on infinite Mach numbers. In practice, the

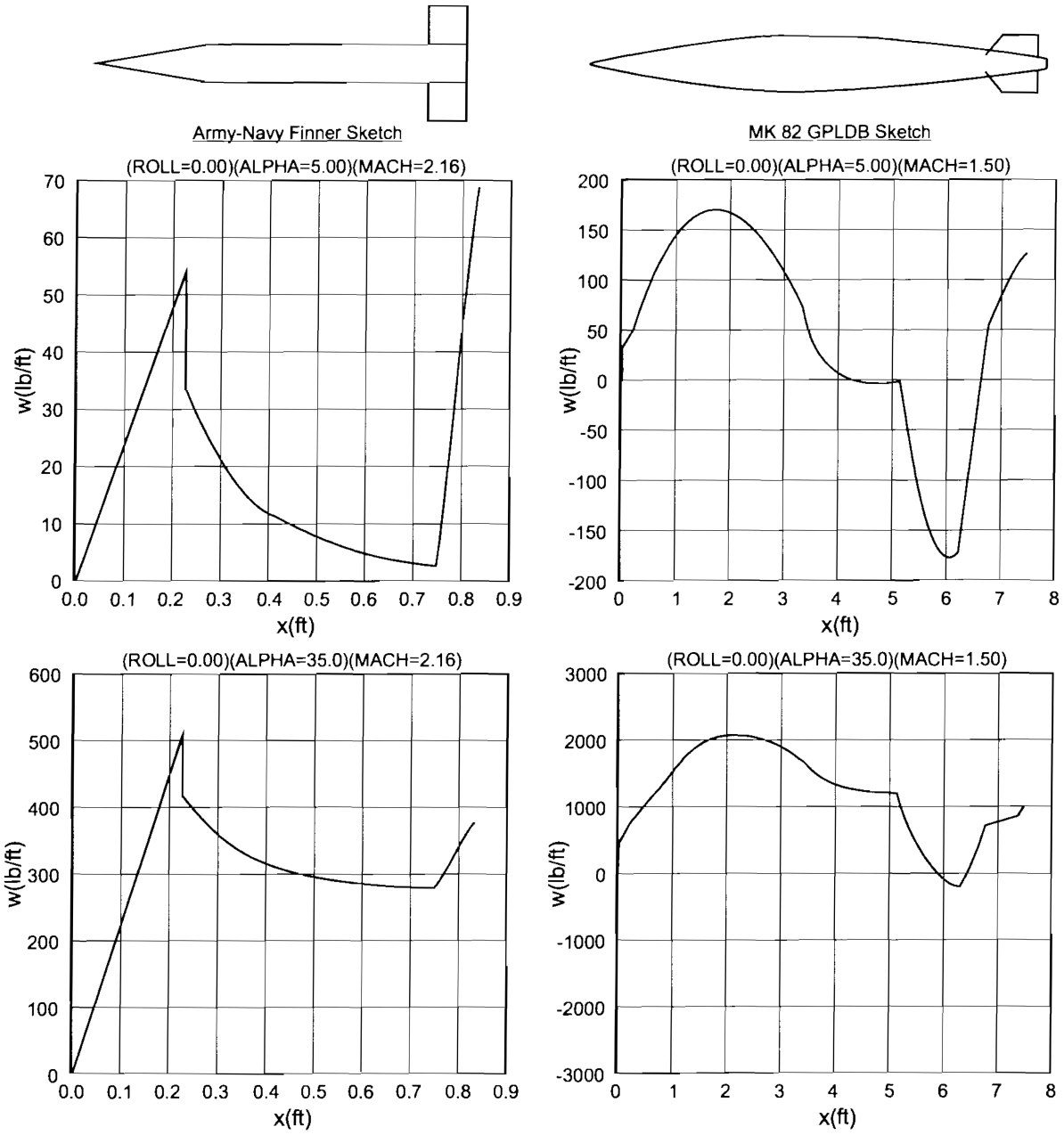

Fig. 3 Local loads on two body–tail configurations at small and large angles of attack.

author has found success in using Eq. (17) down to low supersonic Mach numbers. Also

$$\frac{T_\infty}{T_L} = \frac{1 + \frac{\gamma-1}{2}\mathrm{M}_L^2}{1 + \frac{\gamma-1}{2}M_\infty^2} \tag{18}$$

Substituting Eqs. (10), (17), and (18) into Eq. (15), Eq. (11) becomes

$$\frac{Q_L}{Q_\infty}\frac{V_\infty}{V_L} = \cos\alpha\left[\frac{1 + \frac{\gamma-1}{2}M_\infty^2\cos^2\alpha}{1 + \frac{\gamma-1}{2}M_\infty^2}\right]\left[1 + \gamma M_\infty^2\sin^2\alpha\right] \tag{19}$$

One approach is thus to use Eq. (19) to multiply the pitch damping moment at near 0-deg AOA for a given freestream Mach number and AOA to get the nonlinear value of pitch damping moment. This method is referred to as method 3 of Fig. 1. The zero AOA values of $C_{M_q} + C_{M_{\dot\alpha}}$ come from the AP09 code as modified by the Ref. [19] methods and these values are multiplied by the factors of Eq. (19).

In viewing method 3 of Fig. 1 it is clear it agrees with the AEDC data better than either methods 1 or 2. It is also clear that the reason such a simple formula works so well is the similarity of the nose loading in Fig. 3 in going from low to high AOA. Method 3 tends to average out a lot of the data in Fig. 1, but it follows the general trends of the data. Although not shown, the data of [4] actually go to 85-deg AOA with a maximum in pitch damping occurring around 45-deg AOA and then declining. Equation (19) follows this trend as well. Hence, it is believed Eq. (19) does in fact capture much of the physics of why pitching damping increases with AOA.

The major limitation of Eq. (19) is the use of the Newtonian theory to predict the pressure coefficient. Unfortunately, there are no local slope pressure predictors for low Mach number. As a result, to use method 3 in a robust sense with respect to Mach number, we must find a complimentary factor for lower Mach numbers, which is primarily AOA dependent. To do this, Fig. 4 shows a plot of Eq. (19) versus Mach number for various AOAs. As seen in Fig. 4, Eq. (19) decreases significantly with Mach number. Equation (19) is used down to a Mach number of 1.5, where it is believed the Newtonian theory becomes questionable. From $M_\infty = 1.5$ to 0, it is assumed the value of Eq. (19) goes to 1 in a linear sense. Also of note in Fig. 4 is the fact that Eq. (19) reaches a maximum at $\alpha = 45$ deg and declines to zero at $\alpha = 90$ deg.

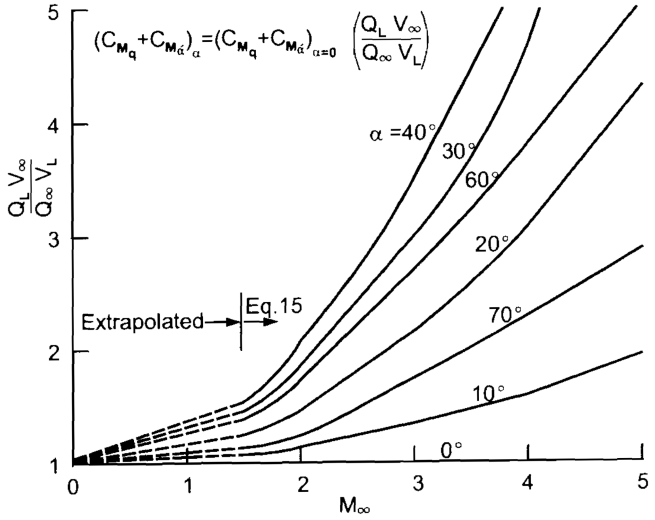

Fig. 4 Approximate relationship to allow pitch damping nonlinearities to be estimated based on $C_{M_q} + C_{M_\alpha}$ at zero AOA.

Both methods 2 and 3 are new or improved methods to predict nonlinear pitch damping. It is unclear, based on the Fig. 1 comparison to wind-tunnel data, which method is best. As a result, both methods will be compared to available wind-tunnel data on other configurations in the Results and Discussion sections before

Method 2 – Use Static Aerodynamics Completely

- Uses all nonlinear static aerodynamics of AP09 and structural loads to distribute body loads
- Very robust in α, M_∞, δ, Φ, number of fins
- Distributes fin loads over 100 equally spaced chordwise locations
- Predicts local body pitch damping
- Has minimum empiricism
- More difficult to implement than Method 3

Method 3 – Uses Quaisi-Time Dependent Wing Alone Solution and Combines with Improved Body Alone Pitch Damping

- Uses all improved body alone pitch damping of AP09 for α = 0 deg
- Uses Quaisi-Time dependent wing alone solution
- Uses a simple method to relate zero α aero to AOA
- More empirical and somewhat less robust (no Φ dependence) than Method 2

Fig. 5 Summary of methods 2 and 3 approaches to predict nonlinear pitch damping moments.

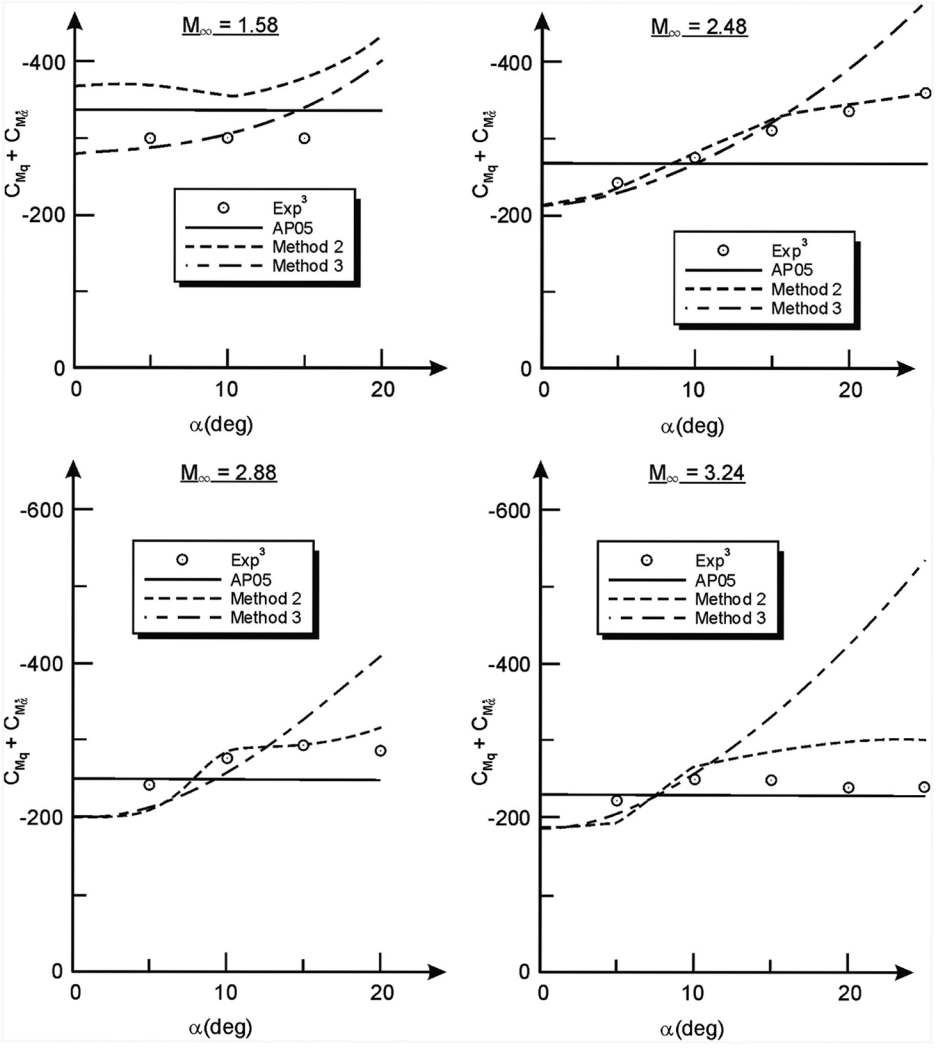

Fig. 6 Comparison of theory and experiment for pitch damping on ANF.

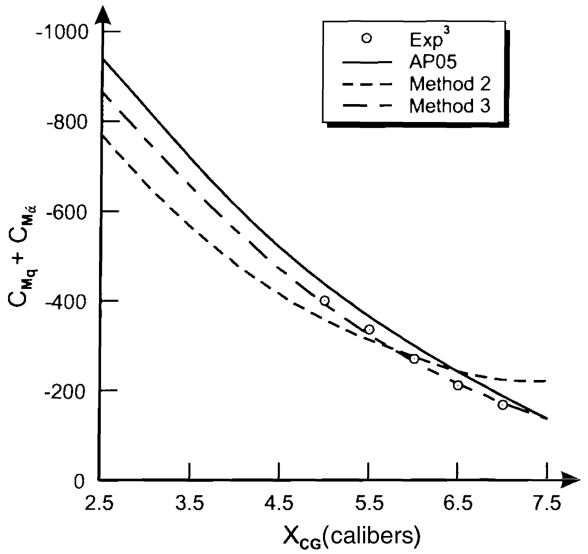

Fig. 7 Comparison of theory and experiment for pitch damping on ANF with various center of gravity locations ($M_\infty = 2.1, \alpha \approx 0$ deg).

any conclusions are drawn. However, it is worthwhile to point out some of the strengths of both methods 2 and 3.

Method 2 is very robust in the sense it will handle all AOAs (0–90 deg) and Mach numbers (0–20) and roll orientations (0, 45 deg), control deflections and multifin options that the AP09 code allows. Method 2 also calculates local body pitch damping moments. It has much less empiricism than method 3 does. On the other hand, it was much more involved and difficult to implement than method 3, even though the AP09 code already had all the nonlinear static aerodynamics and structures loads available for $M_\infty \geq 1.2$.

Method 3 uses the original time-dependent linear solution for $C_{M_{\dot{\alpha}}}$ and rotational pitching rate C_{M_q} from linear theory. Method 3 uses the improvements in pitch damping due to long boattails derived for the AP09 [19]. Method 3 was also much easier to implement than method 2. Figure 5 summarizes the approaches of methods 2 and 3.

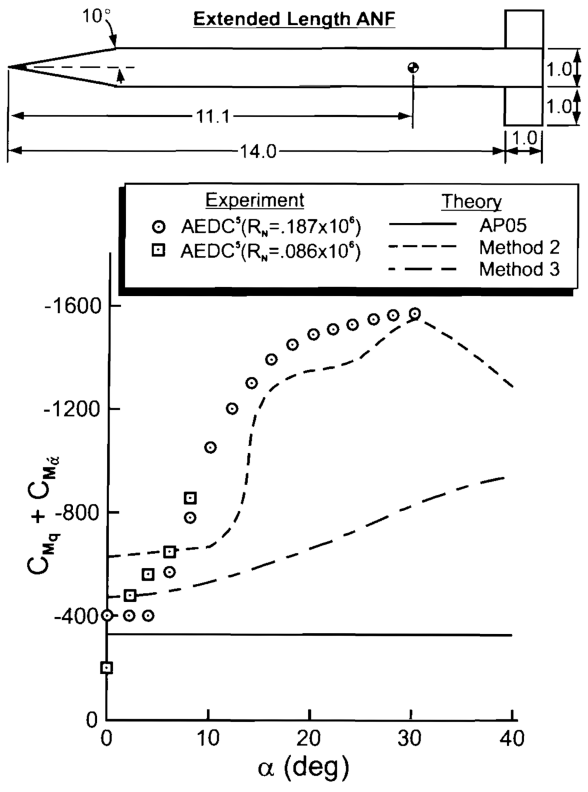

Fig. 8 Comparison of theory and experiment for extended length ANF ($M = 1.96$).

Results and Discussion

Figure 1 showed the results of methods 2 and 3 compared to experimental data for the ANF at about Mach 2.0. Figure 1 illustrated the fact that method 2 compared closer to one set of experimental data than method 3, whereas nethod 3 compared closer to the other set of experimental data than method 2. Both methods 2 and 3 will therefore be compared to the remaining sets of open literature data that the authors were able to find to see if one method can be found to be superior in general to the other method.

Figure 6 compares methods 2 and 3 to the ANF data [3] at $M_\infty = 1.58, 2.48, 2.88$, and 3.24 as a function of AOA. Also shown in the figure are the AP05 results, which are independent of AOA. Note, first of all, the ANF pitch damping data, while varying with AOA, are not highly nonlinear. The reason for the small nonlinearity is the fact the body pitch damping increases with AOA but the wing term decreases with AOA due to the aspect ratio and the fact C_{N_α} of the wing decreases with increasing AOA. The two pitch damping terms tend to offset giving a small increase with AOA for the CG selected. In comparing the AP05 and methods 2 and 3 of the AP09 to experimental data, it is seen that both methods 2 and 3 follow the

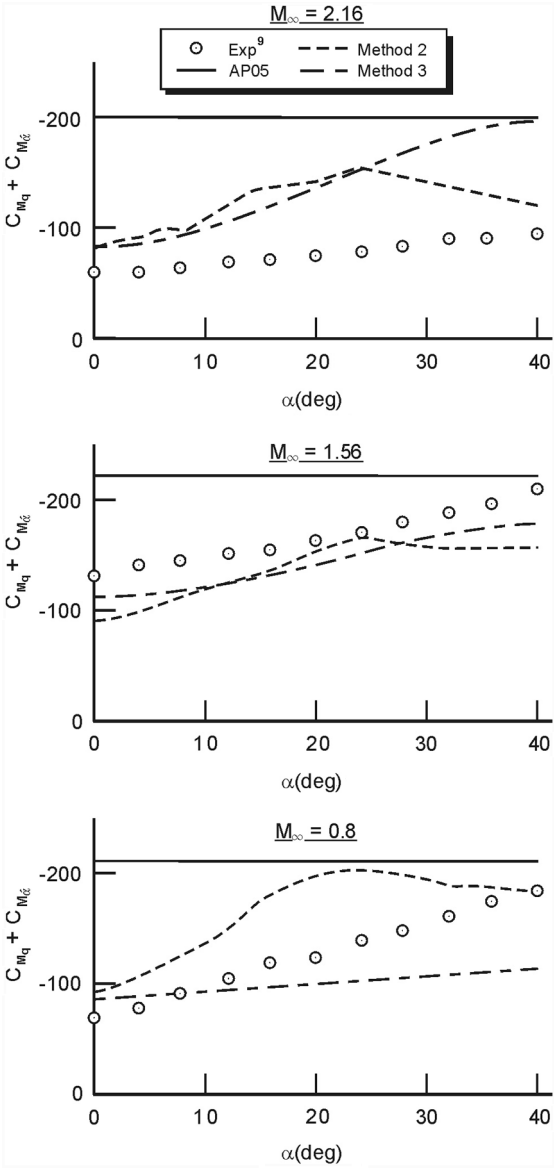

Fig. 9 Comparison of theory and experiment for MK82 low drag bomb.

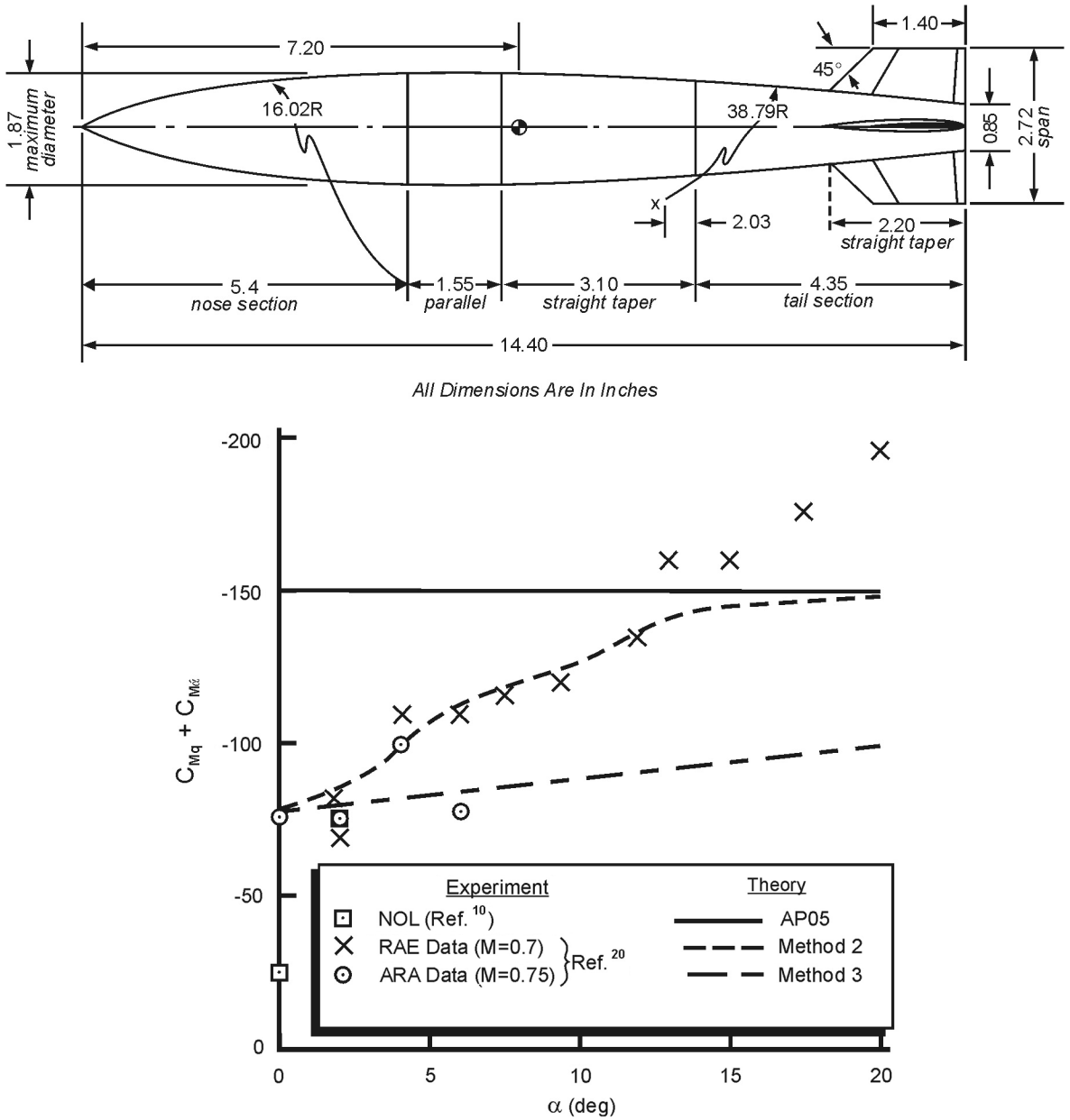

Fig. 10 M823 research store comparisons of theory and experiment for pitch damping.

general trends of the data and the AP05 also gives reasonable values compared to experiment due to the relatively small nonlinearity. Method 2 is probably slightly superior to method 3 in general, particularly at high M_∞ and AOA.

Figure 7 compares the three theoretical approaches to experimental data [3] for the ANF at $M_\infty = 2.1$ and AOA near zero as a function of the CG location. Here it is seen that method 3 is slightly superior to both the AP05 and method 2 compared to experiment [3].

The next case considered is an extended length (15 calibers versus 10 calibers) ANF (see Fig. 8). Experimental data are taken from [4] at $M_\infty = 1.96$. By extending the length of the ANF by 5 calibers, it is seen the pitch damping increases greatly with AOA due to the large body term. It is also seen that method 2, which includes all the nonlinear body loads from the AP09, is clearly superior to method 3 and the AP05.

The third configuration considered is the MK 82 low drag bomb with data taken from [9]. Results are shown in Fig. 9 for $M_\infty = 2.16$, 1.56, and 0.8 to AOA of 40 deg. Here methods 2 and 3 are far superior to the AP05, due in part to the large boattail. Also method 2 is slightly better than method 3 at $M_\infty = 2.16$ and 0.8 and method 3 is slightly better than method 2 at $M_\infty = 1.56$.

The fourth and final configuration where open literature data were found is the M823 research store with data given in [10,22]. Data for the $M_\infty = 0.7$ and 0.75 are shown in Fig. 10 at AOA up to 20 deg whereas Fig. 11 has data at AOA of about 3 deg for Mach numbers 0.6 to 1.1. In Fig. 10, method 2 is clearly superior to method 3 and the AP05. Note the large nonlinearity in pitch damping. The large nonlinearity comes primarily from the tail term where C_{N_α} increases with AOA. Figure 11 clearly shows both methods 2 and 3 are superior to the AP05 and fairly close to experimental data at all Mach numbers. Figure 11 also illustrates the fact that method 2 is roll dependent whereas method 3 is roll independent. The roll dependence of method 2 comes from the difference in body–wing carryover normal force at $\Phi = 0$ versus $\Phi = 45$ deg roll.

Conclusions

Two new methods have been developed to estimate pitch damping at AOA. The first method (method 2) is based on using the nonlinear static aerodynamic loads available in the Aeroprediction Code and the second method (method 3) is based on a new formula derived to relate the zero AOA pitch damping available in the APC to a new AOA. It was found that while method 2 was more robust and slightly

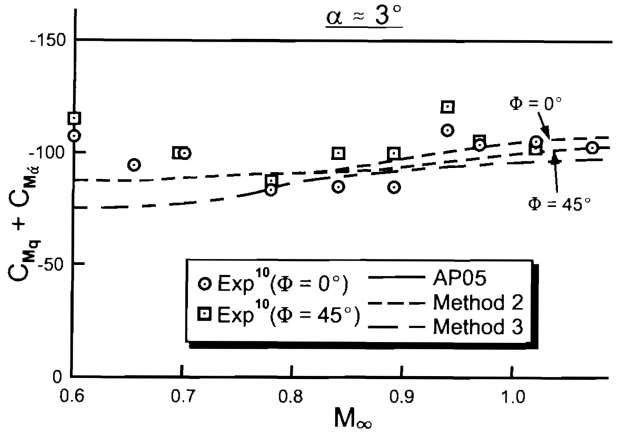

Fig. 11 M823 research store comparisons of theory and experiment for pitch damping.

superior to method 3 when compared to experimental data in most cases, method 3 was superior to method 2 in some cases. Therefore, both methods 2 and 3 will be available in the tabular output of the next version of the APC, the AP09. Method 2 will be available in the plots since it was better than method 3 in most cases.

One of the main issues encountered in assessing the two new methods was the small amount of true pitch damping data and the concerns about wind-tunnel interference effects for the data that were available. A good "truth" set of pitch damping data is clearly needed that has a minimum of wind-tunnel interference issues associated with it. This truth model should be backed up with Navier–Stokes computations so as to minimize any wind-tunnel interference issues.

References

[1] Moore, F. G., "Approximate Methods for Weapon Aerodynamics," AIAA Progress in Astronautics and Aeronautics, Vol. 186, Aug. 2000.

[2] Moore, F. G., and Hymer, T. C., "The 2002 Version of the Aeroprediction Code: Part 1—Summary of the New Theoretical Methodology," NSWCDD/TR-01-108, March 2002.

[3] Shantz, I., and Groves, R. T., "Dynamic and Static Stability Measurements of the Basic Finner at Supersonic Speeds," NAVORD Rept. 4516, Jan. 1960.

[4] Uselton, B. L., and Uselton, J. C., "Test Mechanism for Measuring Pitch Damping Derivatives of Missile Configurations at High Angles of Attack," AEDC TR-75-43, May 1975 (NTIS AD-A009-865, U.S. Department of Commerce, Springfield, VA 22151).

[5] Uselton, B. L., and Jenke, L. M., "Experimental Missile Pitch and Roll-Damping Characteristics at Large Angles of Attack," *Journal of Spacecraft and Rockets*, Vol. 14, No. 4, April 1977, pp. 241–247.

[6] Gillis, C. L., and Chapman, R., Jr., "Summary of Pitch-Damping Derivatives of Complete Airplane and Missile Configurations as Measured in Flight at Transonic and Supersonic Speeds," NACA RM L52K20, Jan. 1963.

[7] Pierens, D. A., "Pitch and Roll Damping Coefficients of the Australian 81 mm Improved Mortar Projectile," DSTO TR-0020, May 1994.

[8] Anderson, C. F., and Carlton, W. E., "Static and Dynamic Stability Characteristics of the Fixed-Fin and Inflatable Stabilizer Retarder Configurations of the MK-82 Store at Transonic Speeds," AEDC TR 75-149, Nov. 1975; also AFATL TR-75-141, Nov. 1975.

[9] Piper, W. D., and DeMeritte, F. J., "Summary of the NOL Investigations to Date of the Aerodynamic Characteristics of the Navy Low Drag Bomb," NAVORD Rept. 5679, Feb. 1960 (DTIC, Cameron Station, Alexandria, VA 22314).

[10] Regan, F. J., Holmes, J. E., and Falusi, M. E., "Pitch Damping Tests of the M823 Research Store with Cruciform and Split-Skirt Stabilizers," NOL TR 65-68, Oct. 1966 (DTIC AD 644804, Cameron Station, Alexandria, VA 22314).

[11] Billingsley, J. P., and Norman, W. S., "Relationship Between Local and Effective Aerodynamic Pitch Damping Derivatives as Measured by a Forced-Oscillation Balance for Preliminary Viking Configurations," AEDC TR-72-25, May 1972 (NTIS, Springfield, VA 22151).

[12] MacAllister, L. C., "The Aerodynamic Properties of a Simple Non-Rolling Finned Cone Cylinder Configuration Between Mach Numbers 1.0 and 2.5," BRL Rept. 934, May 1955 (DTIC, 8725 John J. Kingman Road, Suite 0944, Ft. Belvoir, VA 22060-6218).

[13] Davis, B. S., "Comparison of Aerodynamic Coefficients for the M483A1 and XM898 Projectiles Determined from Transonic Range Data," BRL MR-3999, Sept. 1992 (DTIC ADB168181).

[14] Brown, G. T., and McCoy, R. L., "Free Flight Aerodynamic Characteristics of Three 120 mm Mortar Projectiles: XM 934-HE, XM 930-Illuminating, XM 929-Smoke," BRL MR-3884, Jan. 1991 (DTIC ADB152531).

[15] Robinson, M. L., "The Estimation of Pitch Damping Derivatives of Missile Configurations at Subsonic Speeds," WRE TN HSA 144, Jan. 1969 (DTIC AD857732).

[16] Cyran, F. B., and Marquart, E. J., "Pitch- and Yaw-Damping Tests of the AFATL Aerodynamic Data Correlation Model at Mach Numbers 1.75 to 3.0," AEDC TSR-79-V34, Aug. 1979 (DTIC ADB040452).

[17] Uselton, J. C., and Uselton, B. L., "Wind Tunnel Investigation of the Static-Stability, Drag, Magnus and Damping Characteristics of a 105 mm Projectile at $M_\infty = 1.5$ and 1.75," AEDC TR-71-203, Oct. 1971 (DTIC AD888314).

[18] Carroll, C. J., and Groves, R. T., "Pitch Damping of a 0.15 to −1 Scale Model of the Sidewinder 1 C Missile at Mach Numbers of 1.53, 1.76, 2.28, 2.54, and 3.26," NAVORD Rept. 6836, March 1960 (DTIC AD317948).

[19] Moore, F. G., and Moore, L. Y., "Improvements in the Aeroprediction Code for Configurations with Long Boattails," *AIAA Atmospheric Flight Mechanics Conference*, 20–23 Aug. 2007, and *Journal of Spacecraft and Rockets* (to be published).

[20] Chin, S. S., *Missile Configuration Design*, McGraw–Hill, New York, 1961.

[21] McInville, R. M., Moore, F. G., and Housh, C., "Nonlinear Structural Load Distribution Methodology for the Aeroprediction Code," NSWCDD/TR-96/133, Sept. 1996 (NSWC, Dahlgren Division, Dahlgren, VA 22448-5100).

[22] Marsden, P., "Results of Wind Tunnel Tests on the M823 Research Store with Fixed Monoplane Fins," ARA Model Test Note M.25/1, Sept. 1967 (also AD 857732 from Defense Technical Information Center, 8725 John J. Kingman Road, Suite 0944, Ft. Belvoir, VA 22060-6218).

J. Martin
Associate Editor